Letter

Magnetization-induced optical rectification and inverse spin Hall effect for interfacial terahertz generation in metallic heterostructures

Zehan Yao,[1,2] Huarui Fu,[3] Wanyi Du,[1] Yuanyuan Huang,[1,*] Zhen Lei,[1] Caiyin You,[3,†] and Xinlong Xu[1,‡]

[1]*Shaanxi Joint Lab of Graphene, State Key Laboratory of Western Energy Photonics Technology, International Collaborative Center on Photoelectric Technology and Nano Functional Materials, Institute of Photonics & Photon-Technology, Northwest University, Xi'an 710069, China*

[2]*Division of Chemical Physics, Department of Chemistry, Lund University, Box 124, SE-22100 Lund, Sweden*

[3]*School of Materials Science and Engineering, Xi'an University of Technology, Xi'an 710048, China*

(Received 20 March 2021; revised 5 May 2021; accepted 6 May 2021; published 19 May 2021)

Metallic heterostructure as promising terahertz (THz) spintronic emitters has promoted the development of both spintronics and THz science. However, the underlying physics at the metallic interface, such as the nonlinear optical effect, remains unclear. Herein, we present interface magnetization induced THz generation from metallic heterostructure consisting of Heusler alloy CoFeMnSi (CFMS) and Pd thin films. THz generation is ascribed to 35% contribution from the magnetization-induced optical rectification (MOR) and 65% contribution from inverse spin Hall effect (ISHE) based on the pump polarization and sample azimuthal angle dependent measurement. Furthermore, the contribution ratio of the MOR decreases to 12% via lowering the CFMS grown temperature, which is due to the reduced crystalline quality and possible metal to semiconductor transformation in CFMS. Our results not only clarify MOR and ISHE in metallic heterostructure for the scientific field, but they also benefit THz source optimization for the technology field.

DOI: 10.1103/PhysRevB.103.L201404

I. INTRODUCTION

Spintronic THz emitters have stimulated extensive attention due to their qualities of high intensity and broadband THz generation [1], which have been developed as potential ultrabroadband emitters (0.1–30 THz) for THz applications. Most of the spintronic emitters are metallic interfaces consisting of ferromagnetic metal (FM) and nonmagnetic metal (NM) layers, where ultrafast photocurrent and the induced THz emission arise from the spin to charge conversion by inverse spin Hall effect (ISHE) [2]. The intensity of THz generation by ISHE was then optimized by carefully selecting the NM material [3], layer thickness [3], external magnetic field [4], crystal structure [5], and chemical doping [6]. Aside from ISHE, several physical processes based on spintronics also have important contributions to THz wave generation at the FM/NM interface, such as inverse the Rashba-Edelstein effect [7,8]. However, there is an open question of whether the nonlinear optical process happens at the FM/NM interface. Since the nonlinear optical process plays a key role for THz generation in most nonmagnetic materials, this question is important for unveiling the interfacial physics as well as enhancing the THz emission efficiency of the spintronic THz emitter. Although the nonlinear optical process in a FM metal thin film was suggested to be an important contribution to THz generation [9], it has not been fully understood in FM/NM metallic heterostructures.

As an emerging half-metallic ferromagnetic Heusler alloy, CoFeMnSi (CFMS) provides access to investigating interfacial physics at FM/NM interfaces for THz generation. CFMS with half-metallic energy band structure has an open band gap of 1.7 eV in the minority spin subband and a zero band gap in the majority spin subband [10]. The unique band structure gives rise to a high and tunable spin polarization [11,12]. Although Heusler alloys were present to generate either broadband THz signal by ultrafast demagnetization [13] or narrow-band THz signal by coherent spin precession [14], their interfacial physics of the nonlinear optical process still remains to be uncovered. Therefore, constructing metallic interfaces with Heusler alloys and large Hall conductivity NM metals for THz generation is a key step toward unveiling the interfacial physics of the nonlinear optical effect and ultrafast photocurrent in metallic heterostructures based on Heusler alloys.

In this letter, we have studied the THz generation from a metallic interface based on Heusler alloy CFMS and NM metal Pd. At an external magnetic field, magnetization-induced optical rectification (MOR) and ISHE are dominant mechanisms for THz generation from CFMS/Pd. Among them, ∼35% of THz generation amplitude is ascribed to MOR and ∼65% to ISHE. Both MOR- and ISHE-induced THz generation amplitudes are closely related to the CFMS grown temperature that changes the crystalline quality. Among them, the MOR contribution can be further tuned from 35% to 12% by reducing the grown temperature with the potential metal to semiconductor phase transition. Our results present a clarification for MOR and ISHE in metallic interface based on Heusler alloy for THz generation.

*yyhuang@nwu.edu.cn
†caiyinyou@xaut.edu.cn
‡xlxuphy@nwu.edu.cn

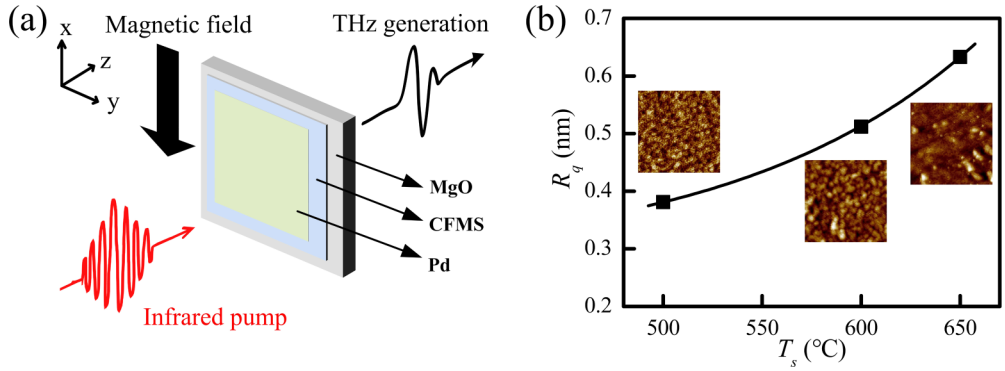

FIG. 1. (a) Schematic of THz generation from the CFMS/Pd interface at an external magnetic field. (b) AFM root mean square roughness of CFMS surface with respect to T_s. Insets are the AFM images of CFMS surface with $T_s = 500\,^{\circ}\mathrm{C}$, $600\,^{\circ}\mathrm{C}$, and $650\,^{\circ}\mathrm{C}$, respectively.

II. EXPERIMENTAL SETUP AND SAMPLE PREPARATION

As illustrated in Fig. 1(a), the THz generation experiments were performed in a transmission configuration. As shown in Fig. 1(a), the infrared pump beam propagating along the z direction was at normal incidence onto the sample with a spot diameter of ~3 mm. The magnetic field $B = 24\,\mathrm{mT}$ was applied along the x axis [Fig. 1(a)], which is parallel to the sample surface and perpendicular to the wave vector of the pump beam. According to the in-plane hysteresis loop behavior of the CFMS, the applied magnetic field in this work can efficiently introduce large in-plane magnetization in CFMS [15]. Further increasing of the magnetic field will not introduce additional effect for the THz emission from the CFMS sample. The experiment was carried out at room temperature and in ambient atmosphere. Since the delayed signal caused by the second reflection in the substrate is too weak as compared to the main signal, we only focus on the main signals in the measurements. More experimental details can be found in our previous work [16].

The 40 nm thick polycrystalline CFMS films were grown on a 0.5 mm thick double side polished MgO (001) substrate by dc magnetron sputtering with 30 W dc power at 3×10^{-5} Pa in an Ar atmosphere using a CFMS target (Hefei Kejing Materials Technology Co., LTD.). A 5 nm palladium (Pd) cover layer was then deposited onto the CFMS film. The samples with growing temperature $T_s = 650\,^{\circ}\mathrm{C}$, $600\,^{\circ}\mathrm{C}$, and $500\,^{\circ}\mathrm{C}$ are named CFMS/Pd-650, CFMS/Pd-600, and CFMS/Pd-500, respectively. Atomic force microscopy (AFM) measurements in Fig. 1(b) suggest the gradually increasing CFMS surface roughness with T_s. Our previous study indicates that the crystallization quality of CFMS increases with the growing temperature T_s and reaches to the best epitaxial growth with the largest grain size on the substrate MgO (001) at $T_s = 650\,^{\circ}\mathrm{C}$ [15]. Furthermore, CFMS thin films with $T_s = 650\,^{\circ}\mathrm{C}$, $600\,^{\circ}\mathrm{C}$ show metallic characteristics at room temperature, while they exhibit semiconductor behavior with $T_s = 500\,^{\circ}\mathrm{C}$ [15]. More details of material preparation and characterization can be found in our previous report [15].

III. RESULTS AND DISCUSSIONS

A p-polarized THz time-domain signal is generated from CFMS/Pd-650 under $0.71\,\mathrm{mJ/cm^2}$ p-polarized illumination as shown in Fig. 2(a), corresponding to a peak to valley value of 11 V/cm, which is 20 times less than that from a 2 mm thick ZnTe (110). The corresponding broadband THz spectrum in the frequency domain is shown in Fig. 2(b). We also measured the THz generation from the bare 40 nm thick CFMS film without Pd covering, of which the THz amplitude is comparable with other Heusler alloys [13] but negligible as compared to the CFMS/Pd. These results suggest that the interfacial effect is the main contribution for THz generation from CFMS/Pd instead of the ultrafast demagnetization effect in bulk. In order to further clarify the THz generation mechanism of CFMS/Pd, we investigate the pump polarization and azimuthal angle dependences of the THz generation, which are effective routes to distinguish nonlinear optical effect from other processes [17]. As shown in Fig. 2(c), the p-polarized THz generation amplitude shows a onefold dependence on the sample azimuthal angle at a fixed pump polarization and external magnetic field direction. The dependence can be fitted by a cosine function, which suggests an isotropic term and an anisotropic term in THz generation. The THz signals from the isotropic and anisotropic contributions have similar bandwidths and central frequencies, but the isotropic THz signal has larger amplitude than that from the anisotropic signal.

For the contribution of the isotropic term, the inverse Rashba-Edelstein effect and Rashba effect are excluded as they mainly display at a trilayer sample containing a Rashba interface or surfaces with Rashba-like splitting [7,8,18], which we did not include in our experiment. ISHE was demonstrated to trigger an ultrafast photocurrent for high intensity THz generation in Fe/Pd interfaces [3]. In our experiment, as CFMS is a ferromagnetic semimetal, ISHE is expected to be the dominant contribution for the isotropic term in THz generation.

In-plane anisotropic THz emission has been ascribed to nonlinear optical effects in various materials. Among them, optical rectification is a second-order nonlinear effect for THz generation at semiconductor surfaces and interfaces with centrosymmetric breaking [19]. At the FM/NM interface, an external magnetic field can cause a second-order nonlinear effect by introducing an in-plane magnetic dipole to break the centrosymmetry [20]. Therefore, optical rectification from either structural- or magnetization-induced centrosymmetric breaking at the CFMS/Pd interface is supposed to be the main contribution to the anisotropic THz generation.

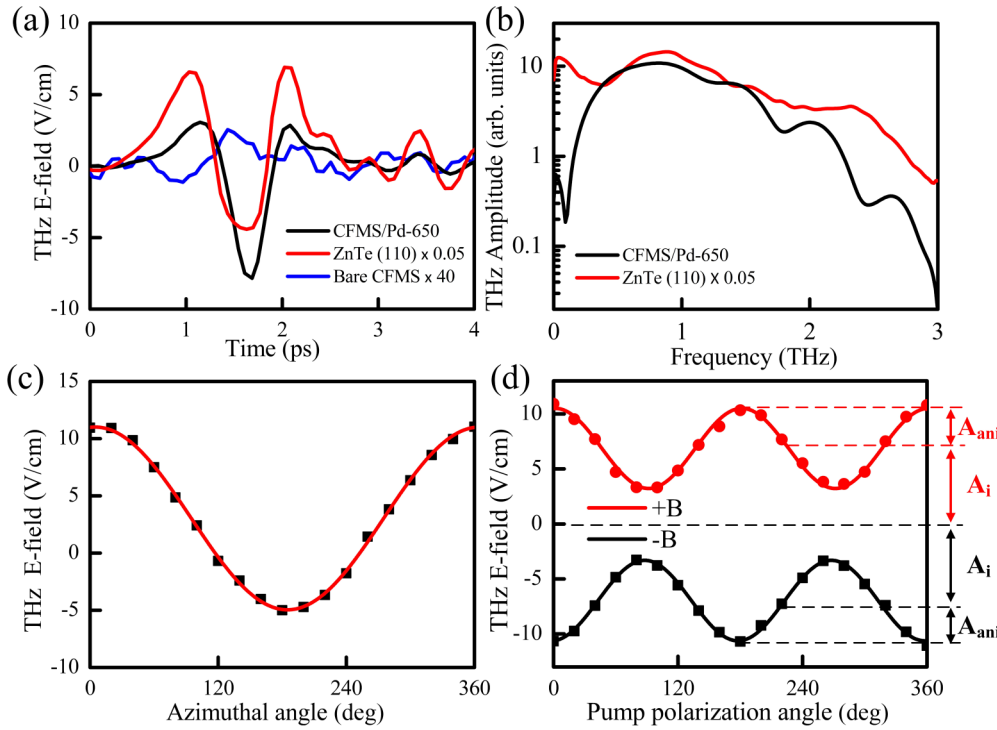

FIG. 2. Comparison of THz generation from CFMS/Pd-650, ZnTe (110) in (a) time domain and (b) frequency domain. THz generation from bare CFMS film [blue line in (a) has been magnified by 40 times] is negligible in our measurement. (c,d) THz generation amplitude from CFMS/Pd-650 with respect to (c) azimuthal angle, and (d) pump polarization angle and external magnetic field direction (+B and −B). Dots are experimental results, and solid lines are the fitted results by cosine function. A_i and $A_{\rm ani}$ refer to isotropic and anisotropic THz generation terms, respectively.

The THz generation from CFMS/Pd as a function of the pump polarization angle under opposite external magnetic field directions is shown in Fig. 2(d). The *p*-polarized THz generation amplitude shows anisotropic dependence with the pump polarization, which can be fitted by a cosine function [16]:

$$E^{\rm THz} = A_i + A_{\rm ani}\cos 2\varphi, \tag{1}$$

where A_i refers to the pump independent isotropic term; $A_{\rm ani}$ refers to the pump dependent anisotropic term; φ refers to the pump polarization angle. The contribution ratio from the anisotropic term can be obtained by $\eta = A_{\rm ani}/(A_i + A_{\rm ani})$. The fitted results shown in Table I suggest the anisotropic and isotropic terms have 35% and 65% contribution ratios to the THz generation amplitude, which indicates a significant nonlinear optical effect in CFMS/Pd. Furthermore, after reversing the applied magnetic field, both the isotropic and anisotropic THz amplitudes flip over without changing the absolute value. These experimental results further confirm the ISHE based on spin superdiffusive transport as the dominant contribution for the isotropic term as reversed magnetic field leads to opposite direction of spin to charge conversion and the consequent ultrafast photocurrent [3]. The mechanism of spin injection in CFMS/Pd is spin superdiffusive transport like the one in conventional Fe/Pt or Co/Pt heterostructures. Spin superdiffusive transport emerges at the material with different electron behaviors between the two spin channels [21] The two spin channels in half-metallic Heusler alloys (such as CFMS) possess zero band gap and open band gap, respectively [11]. This special band structure gives rise to the different electron behaviors between the two spin channels. Therefore, spin superdiffusive transport exists in the CFMS. Other possible spin injection processes are ruled out in CFMS/Pd. (1) Optically induced spin transfer effect happening at a fast timescale (<200 fs) is not a dominant spin injection process in full Heusler materials such as CFMS [22]. (2) Zeeman splitting in the band structure is also excluded due to the small magnetic field (24 mT). (3) Drift photocurrent injection can be excluded due to the lack of external electric field.

TABLE I. Fitting parameters for Fig. 2(d) by Eq. (1).

	+B	–B
Isotropic term	6.86	–6.86
Anisotropic term	3.64	–3.64

Optical rectification is a prevailing method for intense THz generation [23], which is expressed as [19,24]

$$E^{\rm THz} \propto P^{(2)}{}_{\rm OR}(\Omega) = \chi^{(2)}_{\rm str} E(\omega+\Omega)E(\omega) + \chi^{(2)}_{\rm mag} E(\omega+\Omega)E(\omega)M, \tag{2}$$

where P_{OR} is the nonlinear polarization; Ω is the THz frequency; $\boldsymbol{E}(\omega)$ is the incident pump electric field; $\chi^{(2)}_{\rm str}$ and $\chi^{(2)}_{\rm mag}$ are nonlinear susceptibility from structural- and magnetization-induced centrosymmetric breaking, respectively; $\boldsymbol{M}$ is the in-plane dipole moment induced

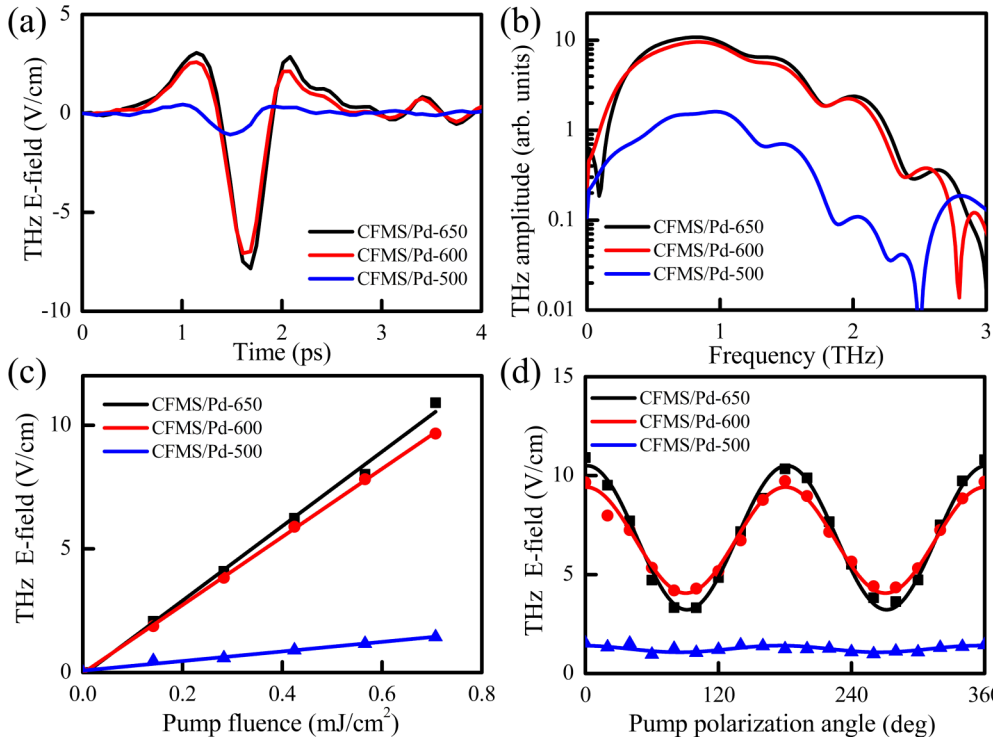

FIG. 3. Comparison of THz generation from CFMS/Pd-650, CFMS/Pd-600, and CFMS/Pd-500 in (a) time domain and (b) frequency domain. (c,d) Comparison of THz generation amplitude as a function of (c) pump fluence, and (d) pump polarization angle. Dots are experiment results and lines are fitted results.

magnetization that is closely related to the external magnetic field. Based on the nonlinear polarization analysis, the THz emission as a function of the pump polarization angle due to the anisotropy from Eq. (2) can be a cosine function as indicated in Eq. (1) [24,25]. According to the fitted results in Table I, the anisotropic THz electric field flips over at the reversing external magnetic field, indicating the dominant contribution from the MOR process i.e., the second term in Eq. (2). Since the THz amplitudes are reversed with identical absolute values under opposite magnetic fields, we conclude that the E^{THz} is proportional to the $\boldsymbol{M}$ in Eq. (2), and the contribution from structural-induced centrosymmetric breaking is negligible. Therefore, ISHE and MOR are identified as main contributions for THz generation from CFMS/Pd. The separation of the isotropic and anisotropic signal contributions is not dependent on certain material systems. This method can also be used to distinguish isotropic and anisotropic THz signal contributions of other magnetic and nonmagnetic materials and structures [9].

In order to gain a deeper insight into the ISHE and MOR at the CFMS/Pd interface, we perform a comparison of THz generation from CFMS/Pd-650, CFMS/Pd-600, and CFMS/Pd-500 with different T_s. As shown in Fig. 3(a), the THz generation amplitude from CFMS/Pd-650 is slightly larger than that from CFMS/Pd-600, while it is significantly larger than that from CFMS/Pd-500. These results are valid in broadband spectra as depicted in Fig. 3(b). The THz amplitude of all CFMS/Pd samples present linear dependences with the pump fluence as shown in Fig. 3(c), which indicate the main contribution of ISHE and MOR in the whole pump fluence range [2,26]. Since the THz generation from CFMS/Pd exhibits anisotropy with the incident polarization [Fig. 2(d)], we compare the THz amplitude from three CFMS/Pd samples with respect to the pump polarization angle. As shown in Fig. 3(d), the THz generation amplitudes from CFMS/Pd-650 are slightly different from CFMS/Pd-600, but significantly different from CFMS/Pd-500 in the whole pump polarization range. To understand the difference, we fit the results by Eq. (1). As shown in Table II, both ISHE- and MOR-induced THz generation amplitude smoothly decreases with reducing T_s from 650 °C to 600 °C, while a sharp decrease of THz amplitude appears with T_s decreasing from 600 °C to 500 °C. Moreover, the MOR contribution decreases from 35% at $T_s =$ 650 °C to 12% at $T_s = 500$ °C, which suggests the close relation between the crystalline quality of the FM film and the MOR contribution to THz generation at FM/NM interfaces according to the surface roughness shown in Fig. 1(b).

The ISHE-induced THz generation with respect to the growing temperature can be understood based on the

TABLE II. Fitting parameters for Fig. 3(d) by Eq. (1). MOR contribution is obtained from $A_{\mathrm{MOR}}/(A_{\mathrm{ISHE}} + A_{\mathrm{MOR}})$.

	CFMS/Pd-650	CFMS/Pd-600	CFMS/Pd-500
A_{ISHE}	6.86	6.74	1.24
A_{MOR}	3.64	2.68	0.17
MOR contribution	35%	28%	12%

theoretical model of ISHE as [3]

$$E^{\mathrm{THz}} \propto \frac{A_p \gamma_{\mathrm{NM}} \lambda_{\mathrm{rel}}}{t_{\mathrm{film}}} \frac{\tanh(t_{\mathrm{NM}}/2\lambda_{\mathrm{rel}})}{n_1 + n_2 + Z_0 \int_0^{t_{\mathrm{film}}} \sigma(z) dz}, \quad (3)$$

where A_p is the absorption fraction of the pump laser; γ_{NM} is the spin Hall angle of the NM material; λ_{rel} is the carrier relaxation length; t_{film} is the thickness of the stacking metal film; t_{NM} is the thickness of the NM layer; n_1 and n_2 refer to the refractive index of substrate and air, respectively; Z_0 is the vacuum impedance; σ is the photoconductivity. More imperfect structure and defects are present in poorly crystallized CFMS with reducing T_s from 650 °C to 600 °C, which gives rise to a higher carrier scattering rate, smaller λ_{rel}, and thus a lower THz generation amplitude according to Eq. (3). With reducing T_s to 500 °C, the CFMS thin film exhibits a semiconductor characteristic, while CFMS at $T_s = 650$ °C and 600 °C exhibits metallic behavior according to our previous study [15]. Spin-polarized photocarrier injection from CFMS to Pd is partially blocked by the Schottky barrier at CFMS/Pd-500 with the semiconductor-metal interface [27]. The same blocking effect is eliminated at CFMS/Pd-600 and CFMS/Pd-650, which are metal-metal interfaces without a Schottky barrier. Hence, ISHE-induced THz generation sharply decreases at $T_s = 500$ °C.

Some factors are demonstrated to remarkably influence the second-order nonlinear optical effect induced THz generation, such as sample orientation [26], pump intensity [26], incident angle [17], material thickness [9], symmetry breaking [28], surface roughness, and material band structure [29]. In our experiment, the pump condition and sample position were fixed, and materials were grown with the same thicknesses. The difference in symmetry breaking between the CFMS/Pd samples mainly comes from the differences in surface morphology and crystallographic quality [24,30]. Surface roughness has been demonstrated to increase the out of plane magnetic dipole moment and decrease the in-plane magnetization by changing the local coordination of FM atoms [24]. Since the THz generation is only sensitive to the in-plane magnetic moment in our experiment; increasing surface roughness ought to reduce the THz generation amplitude from MOR. However, the highest degree of surface roughness appears at CFMS/Pd-650 as indicated in Fig. 1(b), which has the largest MOR amplitude as shown in Table II. Therefore, surface roughness is excluded as a main contribution for enhancing the MOR effect at higher T_s. Except for surface roughness, enhanced crystallization along a certain orientation is able to increase the phase matching efficiency of the second-order nonlinear effect in polycrystalline isotropic materials [31]. As shown in Table II, MOR-induced THz generation amplitude gradually increases with T_s, indicating a gradually enhanced crystallization with T_s [15]. However, MOR-induced THz generation amplitude sharply diminishes to almost zero by reducing T_s to 500 °C, which is incompatible with the prediction by surface roughness, crystallization, and average grain size. With the decrease of T_s to 500 °C, the introduction of surface states and chemical element disorders during the sample preparation process may significantly change the CFMS band structure [32–34], which transforms the CFMS from metal to semiconductor behavior [15]. Consequently, the variation of the CFMS band gap changes the second-order nonlinear effect at the CFMS/Pd interface [35], which is reasonably inferred as the main mechanism for the sharp difference in MOR amplitude between CFMS/Pd-600 and CFMS/Pd-500.

IV. CONCLUSION

We have observed THz generation from a metallic interface consisting of a 40 nm thick Heusler alloy CFMS and 5 nm thick Pd. The THz generation amplitude from CFMS/Pd is dependent on the sample azimuthal angle and pump polarization angle, which suggests a 35% contribution ratio of THz generation from MOR and 65% from ISHE. The THz generation from both MOR and ISHE closely relates to the crystal growing temperature, which changes the crystalline quality and causes the transformation from metal to semiconductor behavior in CFMS. As a result, the MOR contribution decreased from 35% to 12% with the decreasing growing temperature. Our results not only clarify MOR and ISHE as the mechanisms for THz generation from a metallic interface based on a Heusler alloy, but also raise the potential of THz emission spectroscopy for exploring the interfacial physics including magnetization, spin to charge conversion, nonlinear optical processes, and so forth.

ACKNOWLEDGMENTS

This work was supported by National Natural Science Foundation of China (Grants No. 12074311, No. 12004310, No. 11774288, and No. 51771145), the NSFC-ISF Joint Research Program (Grant No. 51961145305), Natural Science Foundation of Shaanxi Province (Grants No. 2019JC-25 and No. 2020JQ-567).

[1] J. A. Fülöp, S. Tzortzakis, and T. Kampfrath, Adv. Opt. Mater. **8**, 1900681 (2019).

[2] T. Kampfrath, M. Battiato, P. Maldonado, G. Eilers, J. Notzold, S. Mahrlein, V. Zbarsky, F. Freimuth, Y. Mokrousov, S. Blugel, M. Wolf, I. Radu, P. M. Oppeneer, and M. Munzenberg, Nat. Nanotechnol. **8**, 256 (2013).

[3] T. Seifert, S. Jaiswal, U. Martens, J. Hannegan, L. Braun, P. Maldonado, F. Freimuth, A. Kronenberg, J. Henrizi, I. Radu, E. Beaurepaire, Y. Mokrousov, P. M. Oppeneer, M. Jourdan, G. Jakob, D. Turchinovich, L. M. Hayden, M. Wolf, M. Münzenberg, M. Kläui *et al.*, Nat. Photonics **10**, 483 (2016).

[4] D. W. Yang, J. H. Liang, C. Zhou, L. Sun, R. Zheng, S. N. Luo, Y. Z. Wu, and J. B. Qi, Adv. Opt. Mater. **4**, 1944 (2016).

[5] G. Li, R. Medapalli, R. V. Mikhaylovskiy, F. E. Spada, T. Rasing, E. E. Fullerton, and A. V. Kimell, Phys. Rev. Materials **3**, 084415 (2019).

[6] M. Chen, R. Mishra, Y. Wu, K. Lee, and H. Yang, Adv. Opt. Mater. **6**, 1800430 (2018).

[7] M. B. Jungfleisch, Q. Zhang, W. Zhang, J. E. Pearson, R. D. Schaller, H. Wen, and A. Hoffmann, Phys. Rev. Lett. **120**, 207207 (2018).
[8] C. Zhou, Y. P. Liu, Z. Wang, S. J. Ma, M. W. Jia, R. Q. Wu, L. Zhou, W. Zhang, M. K. Liu, Y. Z. Wu, and J. Qi, Phys. Rev. Lett. **121**, 086801 (2018).
[9] N. Kumar, R. W. Hendrikx, A. J. Adam, and P. C. Planken, Opt. Express **23**, 14252 (2015).
[10] V. Alijani, S. Ouardi, G. H. Fecher, J. Winterlik, S. S. Naghavi, X. Kozina, G. Stryganyuk, C. Felser, E. Ikenaga, Y. Yamashita, S. Ueda, and K. Kobayashi, Phys. Rev. B **84**, 224416 (2011).
[11] L. Bainsla, R. Yilgin, J. Okabayashi, A. Ono, K. Suzuki, and S. Mizukami, Phys. Rev. B **96**, 094404 (2017).
[12] K. Inomata, N. Ikeda, N. Tezuka, R. Goto, S. Sugimoto, M. Wojcik, and E. Jedryka, Sci. Technol. Adv. Mater. **9**, 014101 (2008).
[13] S. Zhang, Z. Jin, X. Liu, W. Zhao, X. Lin, C. Jing, and G. Ma, Opt. Lett. **42**, 3080 (2017).
[14] N. Awari, S. Kovalev, C. Fowley, K. Rode, R. A. Gallardo, Y. C. Lau, D. Betto, N. Thiyagarajah, B. Green, O. Yildirim, J. Lindner, J. Fassbender, J. M. D. Coey, A. M. Deac, and M. Gensch, Appl. Phys. Lett. **109**, 032403 (2016).
[15] H. Fu, C. You, L. Ma, and N. Tian, Mater. Res. Express **6**, 116119 (2019).
[16] Z. Yao, L. Zhu, Y. Huang, L. Zhang, W. Du, Z. Lei, S. Ajay, and X. Xu, ACS Appl. Mater. Interfaces **10**, 35599 (2018).
[17] Y. Huang, L. Zhu, Z. Yao, L. Zhang, C. He, Q. Zhao, J. Bai, and X. Xu, J. Phys. Chem. C **122**, 481 (2017).
[18] X. Wang, L. Cheng, D. Zhu, Y. Wu, M. Chen, Y. Wang, D. Zhao, C. B. Boothroyd, Y. M. Lam, J. X. Zhu, M. Battiato, J. C. W. Song, H. Yang, and E. E. M. Chia, Adv. Mater. **30**, 1802356 (2018).
[19] Y. Huang, Z. Yao, C. He, L. Zhu, L. Zhang, J. Bai, and X. Xu, J. Phys.: Condens. Matter **31**, 153001 (2019).
[20] V. K. Valev, A. Kirilyuk, F. Dalla Longa, J. T. Kohlhepp, B. Koopmans, and T. Rasing, Phys. Rev. B **75**, 012401 (2007).
[21] M. Battiato, K. Carva, and P. M. Oppeneer, Phys. Rev. Lett. **105**, 027203 (2010).
[22] D. Steil, J. Walowski, F. Gerhard, T. Kiessling, D. Ebke, A. Thomas, T. Kubota, M. Oogane, Y. Ando, J. Otto, A. Mann, M. Hofherr, P. Elliott, J. K. Dewhurst, G. Reiss, L. Molenkamp, M. Aeschlimann, M. Cinchetti, M. Münzenberg, S. Sharma *et al.*, Phys. Rev. Research **2**, 023199 (2020).
[23] F. Blanchard, L. Razzari, H. C. Bandulet, G. Sharma, R. Morandotti, J. C. Kieffer, T. Ozaki, M. Reid, H. F. Tiedje, H. K. Haugen, and F. A. Hegmann, Opt. Express **15**, 13212 (2007).
[24] A. Kirilyuk and T. Rasing, J. Opt. Soc. Am. B **22**, 148 (2005).
[25] R. P. Pan, H. D. Wei, and Y. R. Shen, Phys. Rev. B **39**, 1229 (1989).
[26] Y. Huang, L. Zhu, Q. Zhao, Y. Guo, Z. Ren, J. Bai, and X. Xu, ACS Appl. Mater. Interfaces **9**, 4956 (2017).
[27] L. Cheng, X. Wang, W. Yang, J. Chai, M. Yang, M. Chen, Y. Wu, X. Chen, D. Chi, K. E. J. Goh, J.-X. Zhu, H. Sun, S. Wang, J. C. W. Song, M. Battiato, H. Yang, and E. E. M. Chia, Nat. Phys. **15**, 347 (2019).
[28] M. Cazzanelli and J. Schilling, Appl. Phys. Rev. **3**, 011104 (2016).
[29] X. C. Zhang, Y. Jin, K. Yang, and L. J. Schowalter, Phys. Rev. Lett. **69**, 2303 (1992).
[30] A. Kirilyuk, T. Rasing, M. A. M. Haast, and J. C. Lodder, Appl. Phys. Lett. **72**, 2331 (1998).
[31] B. J. Leroy, S. G. Lemay, J. Kong, and C. Dekker, Nature **432**, 371 (2004).
[32] I. Galanakis, J. Phys.: Condens. Matter **16**, 8007 (2004).
[33] C. Felser, G. H. Fecher, and B. Balke, Angew. Chem., Int. Ed. **46**, 668 (2007).
[34] Y. Feng, H. Chen, H. Yuan, Y. Zhou, and X. Chen, J. Magn. Magn. Mater. **378**, 7 (2015).
[35] S. L. Chuang, S. Schmitt-Rink, B. I. Greene, P. N. Saeta, and A. F. J. Levi, Phys. Rev. Lett. **68**, 102 (1992).